Effect of evaporative surface area on salt efflorescence and subflorescence formation in a given porous material

R. Wijnhorst,[1,*] F. Van der Sloot,[1] L. Pel,[2] and N. Shahidzadeh[1]

[1] *Van der Waals-Zeeman Institute, Institute of Physics, University of Amsterdam, Science Park 904, 1098 XH Amsterdam, Netherlands*

[2] *Transport in Permeable Media, Department of Applied Physics, Eindhoven University of Technology, P.O. Box 513, 5600 MB Eindhoven, Netherlands*

(Received 17 November 2023; revised 16 March 2024; accepted 31 May 2024; published 24 June 2024)

Salt crystallization in composite layered porous materials such as wall paintings, frescoes, tiles, and ceramics can lead to cracks or delamination of the upper layers (paintings and glaze). The resulting open surface areas induce asymmetrical flow of liquid and ions from the heart of the material towards the delaminated evaporative region. By performing drying experiments in truncated cone–shaped sandstone samples as a model system for such flow, we show that for a given volume and a given salt concentration, the size of the evaporative surface (i.e., the large base and the small base) leads to different drying kinetics and salt-crystallization patterns of NaCl. By characterizing the temporal evolution of the ion-concentration profiles by NMR in the liquid during evaporation and by determining the Péclet number over time, we explain this different behavior and the resulting adhesive or nonadhesive efflorescence and subflorescence when the truncated cone–shaped sandstones are dried with either the large base or the small base as the evaporative surface. Fluid transport from a larger region beneath the surface to a smaller, localized evaporative area occurs faster as the surface is approached. This, in turn, combined with the evaporation rate induces greater ion advection, resulting in salt precipitation as nonadhesive efflorescence at the surface. As the damaged area increases, subsurface crystallization interlaced with the efflorescence leads to an adhesive salt crust at the surface. The latter can increase subsequently the chance of mechanical damaging with time. These findings bring new insight into why with aging and the progress of delamination areas the risk of accelerating the deterioration of artworks will also increase.

DOI: 10.1103/PhysRevApplied.21.064055

I. INTRODUCTION

"In time and with water, everything changes," Leonardo da Vinci once wrote [1]. This is especially true for cultural heritage and artworks made from porous structures such as his own mural "The Last Supper." "The Last Supper," being painted on a wall in a convent next to a kitchen, is damaged by a lot of weathering and has been renovated many times, starting as early as a few decades after it was painted in the 16th century [2]. Structural investigations on the mural have shown many cracks in the painting forming preferential pathways for the moisture in the wall to escape and evaporate [3].

If any dissolved ions are present in moisture inside a wall, they will likely precipitate at the places where evaporation occurs. In other words, the salt will most likely crystallize in between the cracks and openings that are formed over time with the aging of the artwork. Murals are not the only forms of cultural heritage that are built from composite porous materials. Aging paintings and ceramics can have craquelure in their top layer, and ceramics and plaster suffer from cracks due to weathering as well. Salt crystallization caused by an interplay between salts, material properties, and environmental changes is one of the main deterioration factors in building materials and cultural heritage [4–8]. It threatens buildings, statues, frescoes, ceramics, paintings, and archaeological objects both inside museums and in the outside environment [9–13]. This process may even be exacerbated by the climate change we are now facing [14].

Over the past few decades, much has been learned about the effects of salt crystallization during evaporation within homogeneous porous materials such as different types of stone and model glass-bead porous media. Different parameters such as pore size, environmental conditions such as temperature and relative humidity, and the effect of different salt types and additives [15–20] have been investigated to better understand the conditions for a given salt to crystallize inside the pore network as subflorescence, or at the surface of the porous material as efflorescence [18]. Both types of crystallization can alter

*Contact author: r.j.wijnhorst@uva.nl

materials and artworks but in different ways. Efflorescence can induce aesthetic problems appearing as white stains, and in the case of a hygroscopic salt due to their deliquescence, the material can get wet more easily at high relative humidity (i.e., summer conditions) [21]. This can subsequently induce other types of problem, such as biological growth on these materials; on the other hand, subflorescence growth, which is accompanied by a crystallization pressure [22,23], can cause cracks and delamination, altering the mechanical properties, and give rise to irreversible loss of material.

Laboratory experiments done with cylindrical samples of various stones or made out of glass beads have shown how the morphology of efflorescence can vary from patchy type (localized assembly of microcrystallites with a porous structure similar to that of a cauliflower) to crusty type, with the formation of an impermeable veil like skin on top of a porous medium (hardly removable) [17,19,24]. Small pore sizes and low relative humidity are more likely to cause crusty efflorescence, which slows down the drying significantly. On the other hand, large pore sizes or high relative humidity causes rather the patchy-type efflorescence [19]. It has also been shown that rewetting-drying cycles either by dissolution (liquid water) or by deliquescence (water vapor) can lead to different recrystallization kinetics for a given salt. In the case of NaCl, multiple dissolution cycles lead to localized larger cauliflower structures as efflorescence, whereas multiple deliquescence cycles lead to the gradual displacement of the salt beneath the surface as subflorescence [17].

However, in most of artworks, we generally face layered materials, such as ceramics, frescoes, tiles, and painted sculptures, in which with aging and alteration cracks or partial delamination in the top, more-impermeable layer can appear; these areas will subsequently form the connection points between the core of the porous material and the outdoor environment for evaporation or wetting. Surprisingly, a careful analysis of these kinds of delamination shows that the visual amount of salt precipitations in these areas varies with the surface area of these evaporative spots [see Fig. 1(b)].

Here we present our results on the effect of fluid transport followed by crystallization across a truncated cone–shaped volume: The impact of fluid transport from a larger region beneath the surface to a smaller, localized evaporative area and vice versa [see Figs. 1(b) and 1(c)] is investigated with different analytical techniques. For this purpose, truncated cone–shaped samples of sandstone were designed as model systems for laboratory investigation [see Fig. 1(d)]. Our results reveal that the amount of salt as efflorescence and the morphology of the latter as well as the amount of subflorescence are controlled by the size of the circular evaporative area for a given volume of sample. By monitoring the ion transport in the sample during evaporation by NMR and by our estimating on the basis of the temporal evolution of the moisture content the Péclet number at the evaporative surface, we can not only show at the laboratory scale but can also explain why smaller areas lead to more efflorescence compared with larger ones. This explanation is in perfect agreement with the salt deposits observed in real cases.

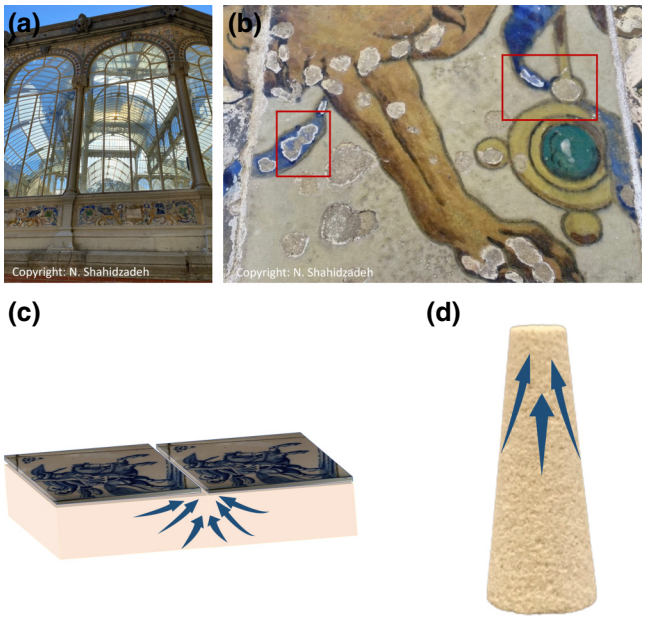

FIG. 1. (a),(b) Tiles in the Palacio de Cristal in Madrid showing damage by salt crystallization. Similarly to laboratory experiments, when a small hole and a large hole in the glaze are next to each other, the small hole shows more salt efflorescence and the crystals start growing on the edge of the hole (both indicated with red squares). (c) Graphical representation of 3D ions and moisture transport during drying of salt solutions in tiles. (d) Cone-shaped Prague-sandstone samples for laboratory study of the process.

II. EXPERIMENT

In the experiments, the drying kinetics and the dynamics of salt (NaCl) precipitation are investigated in real time by our simultaneously using optical microscopy with automated image analysis to monitor the salt precipitation at the evaporative surface of the truncated cones and a balance to register the temporal evolution of moisture content with drying [see Fig. 2(c)].

The truncated cones have a volume of 9.2 cm^3, a porosity of 30%, and average pore-size diameter of 30 μm. They have a height of 50 mm, with a small base with radius r_s = 5 mm and a large base with r_l = 10 mm [see Fig. 2(a)]. The salt solution used in the study is an undersaturated NaCl solution of 1.7M (corresponding to $s = m_i/m_s = 0.3$, with m_i the salt concentration and m_s the concentration at saturation) made by our adding 10 g of NaCl (Sigma-Aldrich, 99%) to 100 g of Milli-Q water. This concentration was

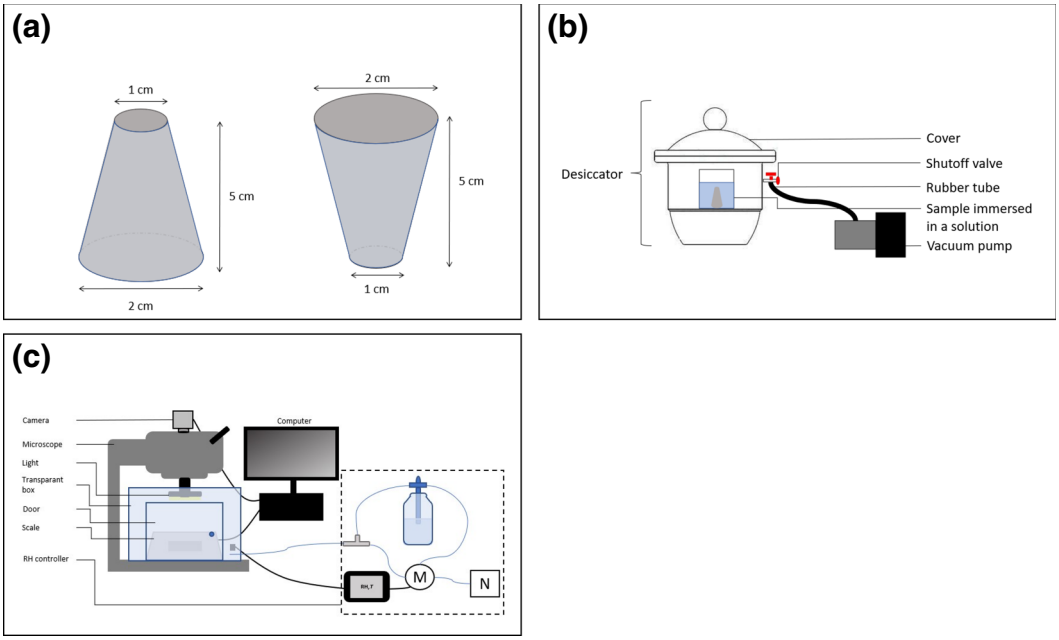

FIG. 2. Setup and samples used during experiments. (a) Cone-shaped porous samples made of Prague sandstone, sealed on the sides and the bottom with Parafilm. (b) Desiccator setup used to saturate the cone-shaped samples with solution. (c) Setup, containing a microscope, a scale, a climate-controlled box, and a camera, used to simultaneously follow the drying process quantitatively and qualitatively. Relative humidity (RH) of 45%. M, solenoid valve; N, nitrogen inlet.

chosen to be representative of realistic situations where salt damage occurs [25,26]. The samples were saturated with the salt solution under a vacuum for 1 h. The samples were weighed before and after the liquid immersion and were subsequently sealed with three layers of Parafilm on the bottom base and lateral side to ensure drying from only the top surface. The evaporation from Parafilm is negligible as the water-vapor permeability of Parafilm is 0.8 g/m^2 per 24 h at a relative humidity of 90%. For experiments that would mean evaporation of 0.002 g per 24 h through the Parafilm for one layer of Parafilm; we covered the sample with three layers. Drying of the samples was then performed in a controlled environmental chamber [relative humidity of (45 ± 5)%, $T = 21\,^{\circ}$C].

The binocular used is a Zeiss Stemi 2000-C microscope with a ring light mounted around the lens. An acA2040-90um/uc camera from Basler is placed on the phototube of the microscope. Pictures are taken every 120 or 600 s. A BCE2241-1S scale from Sartorius is placed underneath the binocular to measure simultaneously the mass of the sample every 60 s. The setup is placed in a climatic chamber where the relative humidity was held fixed at (45 ± 5)% and the temperature was maintained at 21 °C [25,26] by using the system as designed by Boulogne [27] calibrated with a Testo 645 humidity meter. The humidity-controlled box that contains the setup is large: $90 \times 70 \times 60$ cm^3. This fixed the boundary condition for the evaporation at "infinity." That this is reasonable follows if we compare the box size and the evaporative-boundary-layer thickness δ, which is the characteristic length for the evaporative gradient. In Ref. [28] it is shown that δ is approximately to $0.77d$ for water evaporating from a tube, with d the tube's side length. If we assume that the tube is a good approximation for the water flow inside a porous stone, it follows that the diffusion length is a fraction of the pore size d, leading to $\delta \sim 25$ μm, which is indeed much smaller than the box size.

III. RESULTS AND DISCUSSION

In Fig. 3(a) the water saturation over time is plotted and compared for the cone-shaped samples drying with either the large base ($r_l = 10$ mm; dark blue) or the small base ($r_s = 5$ mm; light blue) facing upward. The two drying regimes, consistent with the theory of drying in porous media [29], can be seen in these graphs. The basic phenomenological mechanism of drying in homogeneous porous media without the effect of gravity consists of three distinct regimes: a constant-rate period (CRP), a first falling-rate period, and a second falling-rate period. The constant-drying-rate period during which the capillary velocity is greater than the evaporation rate leads to a homogeneous desaturation of the porous network by capillary equilibration processes and the redistribution of water throughout the whole medium.

The transition to the first falling-rate period occurs when the liquid close to the surface of the porous medium breaks into discontinuous wet patches and leads to a

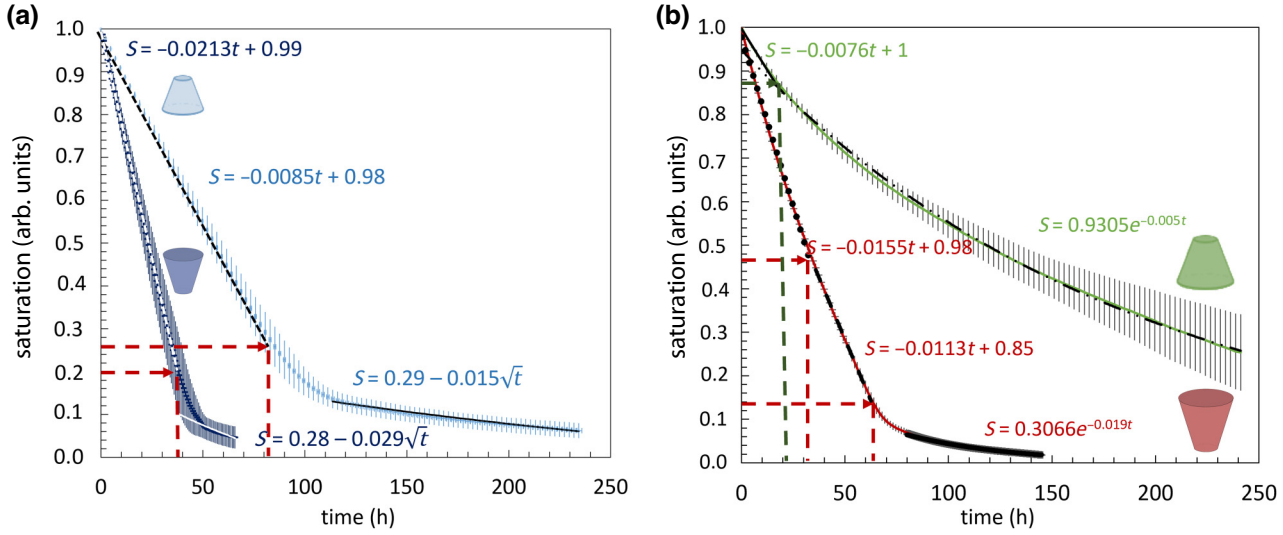

FIG. 3. Liquid saturation during one-dimensional drying in truncated cone–shaped Prague-sandstone samples filled with (a) pure water and (b) 10-wt % NaCl solution as a function of time. (a) Evaporation from the large base facing upward (dark blue) and from the small base facing upward (light blue). Two regimes of drying: a linear fit for the first part (dashed line) and a square-root-of-time fit for the latter part (solid line). The arrows indicate the regime change. The residual saturation and time at the regime change are depicted for both graphs with the dashed red lines. In (b) the graph representing the large base facing upward is shown (red) together with the graph representing the small base facing upward (green) over time. The red line represents the average of three drying curves of different measurements. The green line represents the average of four different measurements. The error bars are the standard deviation. The large base has two CRPs (dotted and dashed lines) followed by an exponential fit for saturation smaller than 0.1 (solid black line). The moisture-content evolution of the small base fits with a linear fit (solid black line), after which the saturation decreases exponentially (dashed black line).

heterogeneous saturation profile near the surface. This results in a dramatic decrease of the drying rate. In this regime the evaporation velocity is greater than the capillary velocity, which in turn is greater than the evaporation velocity inside the porous medium. The drying rate is thus governed by diffusion of vapor through the apparent dry zone of the porous medium. A continuous liquid network is still able to drain toward the interface of highest evaporation throughout drying, regardless of pore size.

The second falling-rate period starts when the liquid does not move inside with the liquid film in the porous medium but simply evaporates. This second falling-rate-period regime is hardly detectable with weight measurements.

In our truncated cone–shaped samples, the water saturation decreases with a constant rate over time (CRP) until residual saturation $S = 0.2$ for the large base and $S = 0.25$ for the small base. The constant-rate period is 2.4 times longer for the large base of the sample than for the small base [the constant-rate period fits with $S = -0.0213t + 0.99$ (dashed white line) for the large base and with $S = -0.0085t + 0.98$ (dashed black line) for the small base]. This is mainly because the evaporative flux is not homogeneous over the evaporative surface area and is higher at the periphery; this is in correspondence with droplet evaporation and the resulting coffee-stain effect and a similar fairy-ring effect in drying of cylindrical porous media [20,30,31]. The evaporation rate is thus proportional to the perimeter [30,31]; in our truncated cone–shaped sample, the ratio between the perimeter of the two bases is a factor of 2, in good agreement with the factor of 2 in the drying rates measured experimentally.

The transition from the CRP to the first falling-rate period occurs for both configurations at a residual saturation of around 20% ($S \sim 0.2$). For the large surface area, the saturation over time fits with $S = 0.28 - 0.029\sqrt{t}$ (solid white line) and for the small surface area fits with $S = 0.29 - 0.015\sqrt{t}$ (solid black line). The square-root-of-t dependence of the liquid saturation in the sample indicates that during this period the drying of the cones is governed by diffusion of the water molecules within the porous medium.

When the samples are saturated with salt solution (1.7M NaCl) [Fig. 2(b)] a remarkable difference can be observed in the drying kinetics between the large base and the small base [Fig. 2(b)]. First, one can notice, in general, that the same cone-shaped samples dry more slowly when saturated with salt solution than with pure water. For both situations, the drying starts with a constant-rate period again differing a factor of 2 [30,31]. It is interesting to note that the large top facing upward has two constant-rate periods: one until $t = 30$ h ($S = 0.48$) and one afterwards until $t = 60$ h ($S = 0.14$). Although this CRP continues for a large surface area (red curve) up to residual saturation of

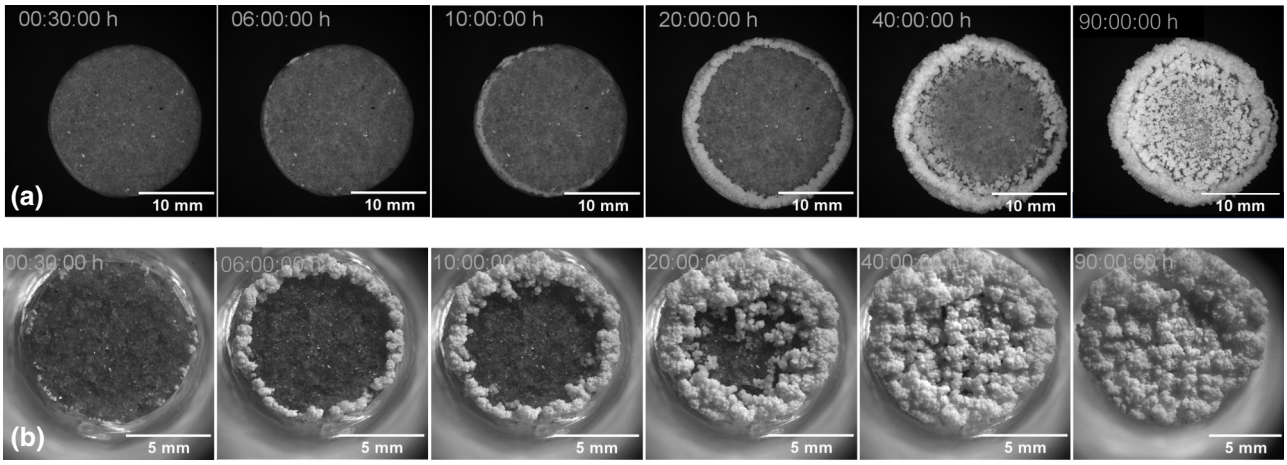

FIG. 4. Top view of the crystallization pattern at the evaporative surface of cone-shaped samples saturated with 10-wt % aqueous NaCl solution when (a) the large surface is facing upward and (b) the small surface is facing upward during drying.

0.14, this first linear regime represents a very short period for the small evaporative surface. At residual saturation of 0.86, there is a transition to an exponential decay of the moisture content over time.

To better understand theses differences, the crystallization patterns were simultaneously followed by our observing the top surface of the cones. When the large surface is facing upward during drying [Fig. 4(a)], we observe that the drying first starts with a ring-shaped growth of salt crystals known as the "fairy-ring effect" [20]. The higher evaporation at the periphery induces the crystallization at the perimeter of the evaporative surface area (see Fig. 3), forming a ring similar to that resulting from the coffee-stain effect or the fairy-ring effect as reported for salt on top of a porous medium [20,31]. This is during the first CRP as depicted in Fig. 3(b). After the fairy-ring formation, the crystallization proceeds with the centripetal colonization of salt crystals, similar to what was observed by Eloukabi *et al.* [19] and Dueñas Velasco *et al.* [32]. This is during the second CRP as depicted in Fig. 3(b). During evaporation, cycles of wetting and drying of the precipitated crystals at the surface can be observed (see Video 1). This is because the crystal precipitation on the top, called "efflorescence," forms a porous medium itself with pores smaller than the stone itself [17] [see Fig. 5(c)]. Because of capillary rise, this porous efflorescence structure can suck up by capillary pumping the salt solution towards the outer layer of this salt layer, where the evaporation is the highest and salt precipitation can continue at the outer surface of the salt crust [18,33]. In our experiments where the large cone base is facing upward, after approximately 60 h, which corresponds to a residual saturation of 0.14, the efflorescence stays white, which indicates that it is dry, and does not show further liquid imbibition anymore (wet stage). From that moment the efflorescence pattern stops evolving at the surface and remains unchanged. The exponential decay of the evaporation becomes relevant at this time (after approximately 60 h), forming the third regime in the drying curve. The transition to the exponential drying regime is related to the increase of crystallization with time in the upper layer of the subsurface as the sample has a lower saturation, which in turn decreases the evaporative surface area [17]. At the end of drying, the efflorescence is strongly adhered to the large surface of the cone and is hardly removable by a brush. Scanning-electron-microscopy (SEM)

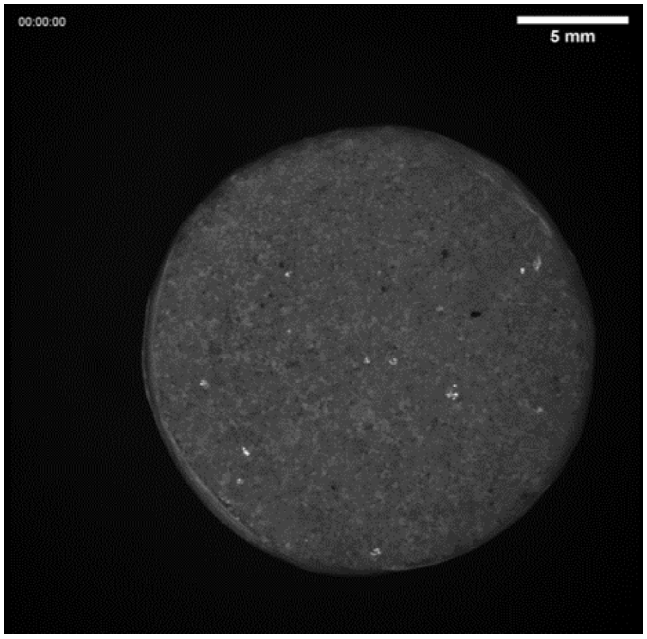

VIDEO 1. Top view of the crystallization pattern at the evaporative surface of cone-shaped samples saturated with 10-wt % aqueous NaCl solution when the large surface is facing upward during drying.

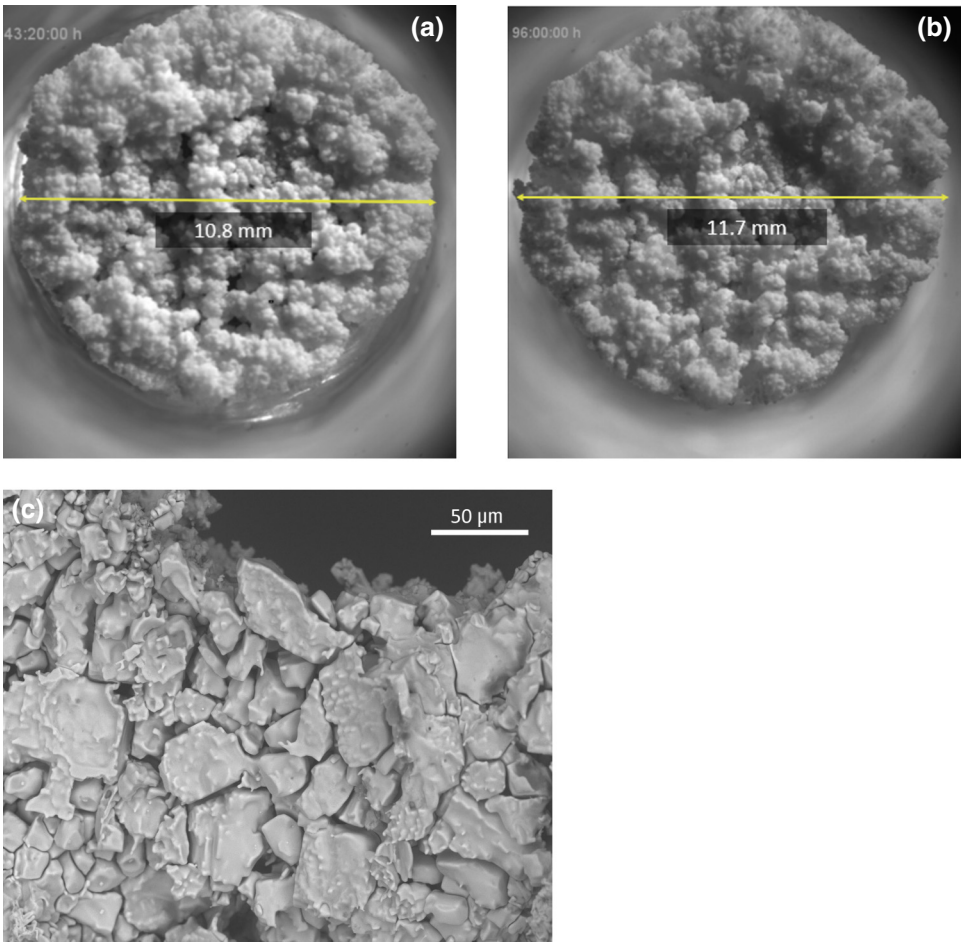

FIG. 5. Self-lifting behavior of the salt crust on the top of a cone-shaped sandstone sample filled with 10-wt % aqueous NaCl solution during drying with the small base facing upward. (a),(b) Top view where the expansion of the salt crust during drying is shown. (c) SEM image of the intersection of the porous salt crust formed on the top of the cone, showing that the salt crust forms a porous medium itself that can suck up solution during drying.

images (obtained with a TM300 tabletop microscope from Hitachi) of the large evaporative surface of the cone show that although the sandstone grains are covered with a layer of salt, the shape of the grains and the pore space are still recognizable. The pores remain open during drying [Fig. 6(e)]. When the evaporative surface is the small base of the truncated cone–shaped samples, we observe the fairy-ring effect as well [Fig. 4(b)] [19,32]. Here the efflorescence clusters, similar to cauliflower structures [16], appear much earlier in time [Fig. 4(b)] and grow to a larger size. At the very beginning of drying, before the ring is formed, a short constant-rate period is observed [Fig. 3(b)]. Once the ring of crystals is completed, again centripetal precipitation continues to cover the whole surface, making a barrier for the direct access of the solution to the air, which slows down the evaporation. Such dynamics of efflorescence leads to an exponential decay of the drying rate with time as the evaporative surface rapidly becomes smaller with time, as shown by Desarnaud *et al.* [17]. It should be pointed out that for the same liquid volume, the reduction of the free surface for evaporation is consequently achieved much earlier for the small base than for the marge base being the evaporative surface. The moment when the whole small surface is covered with salt clusters corresponds to a time of approximately 40 h and a residual saturation of 0.8. Further evaporation and crystallization surprisingly lead to the lift-up of the whole efflorescence crust from the surface of the cone [see Figs. 5(a) and 5(b) and Video 2]. Such lifting up shows that the location of salt precipitation is changing from the top surface of the crust (which remains unchanged) to the bottom layer of the crust. In Fig. 6(a) it can be seen that the efflorescence crust grows several millimeters above the cone surface but can be removed very easily, i.e., there is very weak adhesion to the surface of the stone. SEM images and profilometry scans of the bottom of the crust reveal pillars (legs) of salt crystals [see Figs. 6(c) and 7]. This is very reminiscent of the self-lifting of NaCl crystals from evaporating

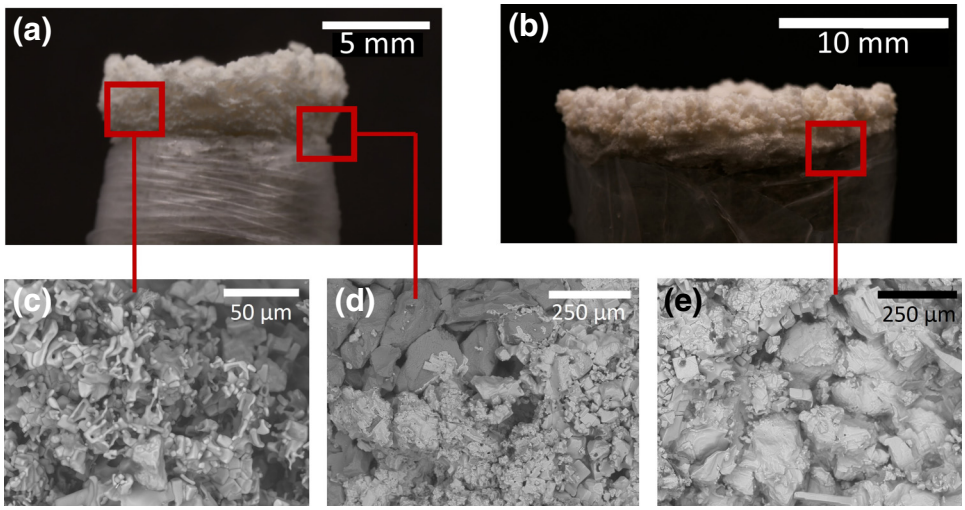

FIG. 6. Side view of dried cone-shaped samples initially filled with NaCl solution (10 wt%): (a) small base and (b) large base as the evaporative surface. SEM images taken from (c) the bottom of the removed salt crust showing "legs" of salt that lift the crust up from the small evaporative surface, (d) leaving a partly-salt-free area at the surface. (e) Surface of the large base showing that although the quartz grains are covered with a tight layer of salt, the pores remain open.

droplets on hydrophobic surfaces due to the formation of salt-crystal pillars [34].

As shown in Fig. 5, the salt crust that forms on the top of the cone is a porous network by itself that by capillary pumping is wetted by the salt solution during the early stage of drying. As we do not observe any crystallization on top of the crust after 50 h, we expect that the outer surface of the crust at this point is not hydraulically connected with the salt solution anymore (see Fig. 8 and Video 2). Subsequently, crystallization occurs in the liquid films beneath the crust at the top of the sandstone surface, accounting for the lifting of this crust from below by the pressure of growing crystals [17] (see Fig. 8). This locally detaches the crust from the surface of the stone, inducing an area with some salt-free zones with a collective macroscopic effect that translates into weak adhesion of the entire efflorescence crust to the surface [Figs. 6(c) and 6(d)]. The whole macroscopic crust can be subsequently detached and removed very easily.

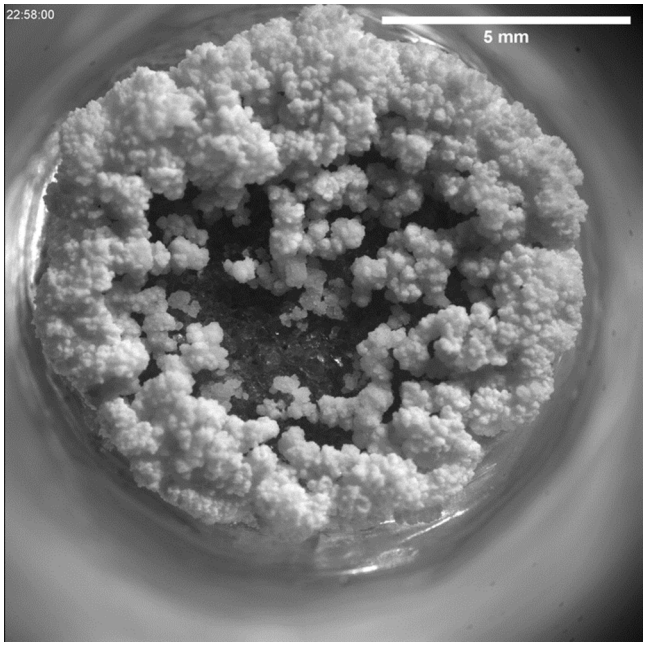

VIDEO 2. Top view of the crystallization pattern at the evaporative surface of cone-shaped samples saturated with 10-wt% aqueous NaCl solution when the small surface is facing upward during drying.

To better understand the relation between the crystallization pattern and the drying kinetics for truncated cone–shaped samples dried with different evaporative surface areas, we have to examine the ion transport during evaporation. The Péclet number characterizes the advective transfort and diffusive transport in a porous medium and the dominance of one over the other. The Péclet number gives the ratio between upward advective transport and downward diffusive transport of the ions during drying [35–37] [Eq. (1)]:

$$\mathrm{Pe} = \frac{UL}{D^*}. \tag{1}$$

As it depends on the velocity of the flow field and a characteristic length L_{char} of the system, it is an efficient way in fluid-mechanical problems to determine the relative importance of advective flux with respect to diffusive flux. The Péclet number for our measurements (see Fig. 9) is calculated over time by our taking the derivative of the average

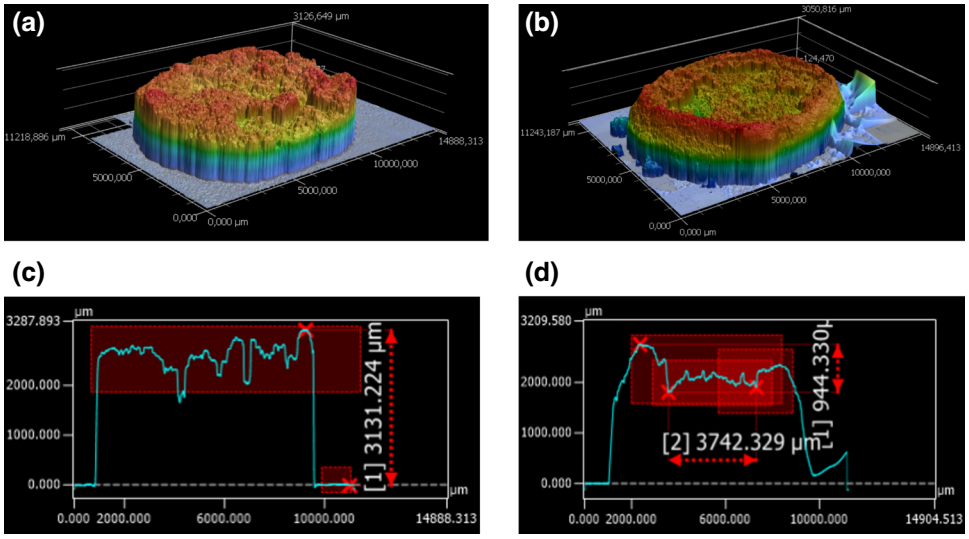

FIG. 7. Profilometry scans of the salt crust after drying on the small surface of the cone. (a),(c) Top scan of the salt crust, where the height of the crust and the upper structure is visible. (b),(d) Bottom scan of the salt crust, where it can be seen that the sides are higher, and the leg structure of the salt crystals is visible. (a),(b) Full 3D scan and (c),(d) line measurements of the crust.

drying curves (g/s) from our experiments every hour and dividing this by the evaporative surface area to get the advection speed U in meters per second. In the experiments, we measured the mass change of the moisture content over time. From the m-versus-t curves, we calculated an average drying curve for each geometry (experiments where the large base is facing upward and experiments where the small base is facing upward). To calculate the Péclet number, an advection speed in meters per second is needed to account for the upward liquid transport. We assumed that in our experiments only water left the sample during the evaporation and that the measured mass is the mass of water. With the density of water, we were able to convert the measured mass change over time to a volume change over time (cubic meters per second). We assumed that for the infinitesimally small distance above the interface between the cone and its environment that the water molecules leave the cone only in the direction perpendicular to the stone surface of the cone. Knowing the volume change in cubic meters per second and the evaporative surface area of the cone in square meters, we were able to estimate the advection speed in meters per second with which the water leave the sample by dividing the change in volume by the evaporative surface area. We have used this evaporation rate in meters per second as U.

L is the characteristic length of the transport, in this case the length of the cone (5 cm), and D^* is the diffusion coefficient (1.5×10^{-5} cm/s) of the ions in our porous material [38–41]. As we show in the drying curves [Fig. 3(b)], due to the blocking nature of the efflorescence in the case of the small base facing upward, the evaporative surface area changes, explaining the exponential drying behavior. From Ref. [17] we know that

$$\frac{dm}{dt} = -cA. \tag{2}$$

For an evaporating drop, an analytical solution exits that gives the evaporation rate in terms of the molar volume, the temperature, and the diffusion coefficient of the water in the vapor phase, since transport through the vapor phase is the rate-limiting step. In this case, the evaporation rate is proportional to the radius (perimeter) of the drop because of the evaporative singularity at the edge [31]. For a porous surface, the reasoning is the same: the evaporation is limited by diffusion, but now the ratio of the surface area to

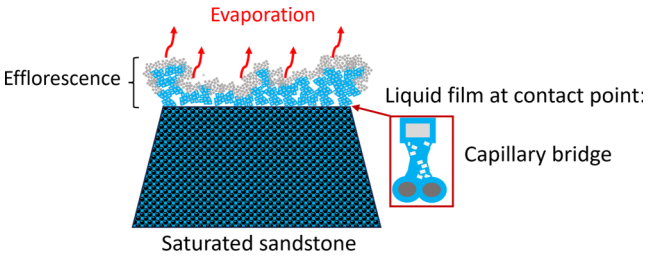

FIG. 8. Top surface of the truncated cone–shaped sample saturated with NaCl solution with the small base facing upward, where the salt efflorescence crust is partially formed. The liquid is indicated with blue. The blue crystals in the crust indicate crystals that are wetted with the salt solution, and the gray crystals correspond to the dried region without a liquid film. Evaporation from the top is indicated with red arrows. Crystallization in the capillary bridges beneath the crust (enlargement in the red square) causes the formation of salt legs beneath the crust, lifting the whole efflorescence from the sandstone surface.

the perimeter length has to be taken into account, so that as observed experimentally dm/dt is proportional to the surface area A. So the constant c is given by the diffusion coefficient and the total perimeter length of the liquid on the porous medium, which gives an extra length scale in the problem, which is the pore size of the porous medium.

Furthermore, we know that

$$\frac{dA}{dt} = \alpha \frac{dm}{dt}. \tag{3}$$

This leads to

$$\frac{d^2m}{dt^2} = -c\alpha \frac{dm}{dt}. \tag{4}$$

The constant α is given by the supersaturation exceeding unity for secondary nucleation: the faster the rate at which supersaturation reaches unity, the faster the crystals will grow and block the pores. The supersaturation is given by the rate of loss of water [15].

The solution of this equation is

$$m(t) = m_0 e^{-c\alpha t}. \tag{5}$$

From the linear fit in the first regime for our data, we were able to calculate dm/dt by making a linear fit at the point before crystallization starts ($dm/dt = -3 \times 10^{-6}$). Knowing the surface area of the small base ($A = 0.79$ cm^2), we can calculate the constant c ($c = 3.8 \times 10^{-6}$). From the exponential fit to our data and knowing m_0, we can estimate the constant α ($\alpha = 0.3625$). Given that

$$\frac{dm}{dt} = -cm_0\alpha e^{-c\alpha t} \tag{6}$$

and

$$\frac{dA}{dt} = \alpha \frac{dm}{dt}, \tag{7}$$

we can estimate the change in evaporative surface area over time by

$$\frac{dA}{dt} = -cm_0\alpha^2 e^{-c\alpha t}. \tag{8}$$

This gives

$$A(t) = m_0\alpha e^{-c\alpha t} + X. \tag{9}$$

Knowing $A_0 = 0.79$ cm^2, we find $X = -0.12$. This variable surface area $A(t)$ is used in the case of drying with the small base facing upward. In the case of the large base facing upward, we observe from the SEM images in Fig. 6(e) that the efflorescence is a thin film, leaving the pore space open. The fact that this efflorescence is nonblocking is confirmed by the constant drying rate of the sample until a saturation S of 0.14.

Upward advection of the ions is dominant in case the Péclet number is larger than 1 [35–37]. This causes a gradient in the salt concentration, with a higher salt concentration at the top of the sample and inducing ions to crystallize from solution as efflorescence on the evaporative surface of the cone. When the diffusion of ions is dominant, the salt concentration is more evenly distributed inside the sample, causing more-dispersed crystallization in the stone, leading to subflorescence (crystallization within the pore) upon evaporation.

It is interesting to note that in Fig. 9 for the same drying conditions, the Péclet number differs significantly between the two evaporative surfaces of the cone-shaped samples. When the large base is facing upward (red curve) the initial Péclet number starts at a lower value (1.5), whereas evaporation from the small base (green curve) leads to an initial Péclet number of 2.7. The advection of ions is therefore more dominant in the latter case. This explains why the precipitation of the salt efflorescence as a ring starts much earlier (after $t =$ 30 min) [Fig. 4(b)] than with the large evaporative surface area (after $t = 6$ h). In both cases this is a remarkable early start of efflorescence growth if we take into account that the salt solution in the sample is undersaturated ($S = 0.3$). Because of the high advection of ions, supersaturation is reached locally at the evaporative surface very quickly for both configurations of the cone.

Using the variable expression for the surface area $A(t)$ in the calculation for the Péclet number, we find that when the small base is facing upward, the Péclet number stays above 1.5 (Fig. 9) during the whole drying time. This high advective flux explains the large amount of salt coming out of the sample and precipitating as efflorescence.

To confirm the ion distribution over time as explained by the estimations of the Péclet numbers, NMR was used to investigate the transport of the moisture and ions inside the cones by our measuring the concentration profiles over time. In a constant magnetic field, the magnetic field of nuclei can be manipulated by radio-frequency pulses. This happens when the oscillation frequency matches the resonance frequency of the nuclei. The manipulation of the nuclei results in a spin-echo signal. NMR is a resonance effect in which the resonance condition for the nuclei is given by $f = \gamma B_0$, where f is the frequency of the radio-frequency field, γ is the gyromagnetic ratio, and B_0 is the applied magnetic field [35,42,43]. The resonance condition allows NMR to be used to recognize certain nuclei.

Air with a relative humidity of 45% is continuously blown over the free surface of the sample. The frequency of the rf coil is set to 33 MHz, which corresponds to the resonance of the H nuclei [43]. The spin-echo signal coming from the part of the sample closest to the center of the rf

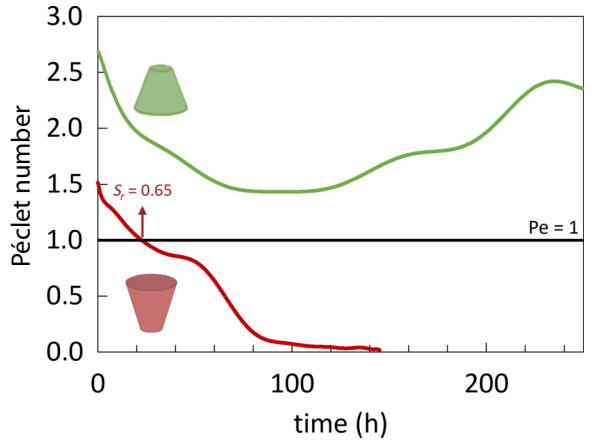

FIG. 9. Evolution of the Péclet number over time for the large base (red line) and small top (green line). The equilibrium between advective and diffusive transport of the ions is depicted with the solid black line. The Péclet number was calculated by taking the derivative of the curve fitting the average curve of multiple measurements (three measurements for the large base, four measurements for the small base) every hour. The arrow depicts the liquid saturation at the time the Péclet number drops below one in case of the red curve. Here, r stands for residual, so S_r is residual saturation.

coil is measured. Then the frequency of the rf coil is set to 9 MHz, which corresponds to the resonance frequency of the Na nuclei [43]. Now the spin-echo signal for the Na nuclei is measured. When the signals for the H nuclei and the Na nuclei are determined, the sample is moved vertically by a stepper motor and then again the signals for the H nuclei and the Na nuclei are determined. This is done until the entire moisture and Na profiles are determined. Both the H signal and the Na signal are proportional to the moisture content and the Na content. It should be noted that no signal is obtained from NaCl crystals as the relaxation time is too short for the echo times used in these experiments. For the analysis of the concentration profiles, we divide each Na profile by the corresponding H profile. By equating the first profile with the initial salt concentration introduced in the cone, we are able to calculate all the concentration profiles over time (Fig. 10).

From these NMR profiles in both samples, we also recognize the concentration gradient at the evaporative surface as predicted from the high Péclet numbers already at the start of the experiments: both samples show a concentration peak towards 6M (the solubility of NaCl) at the initial stage of evaporation at the surface of the sample although the concentration of the initial salt solution used is far below saturation.

When the small base of the cone is facing upward with water evaporation [Fig. 8(b)], the ion concentration increases homogeneously (although it stays below the solubility of sodium chloride) over the height of the sample except at the evaporative surface (position 5 cm), where a sharp increase of concentration can be seen. This sharp peak of ions at the surface is also an indication of the location where salt precipitation is happening, i.e., on the top surface just outside the cone.

When the large base of the cone is facing upward, in addition to the sharp increase of concentration at the surface, further drying leads to the gradual increase of the salt concentration 1.5 cm beneath the evaporative surface (position 3.8–5 cm), leading to a second ion-concentration area. This is also in a good agreement with the evolution of the Péclet number, which becomes lower than 1 after 20 h, meaning that diffusion of ions in the sample becomes more dominant than advection to the surface. From the drying curves in Fig. 3(b) and the Péclet number over time (Fig. 9), it can be seen that the formation of this second concentration region corresponds to the start of the

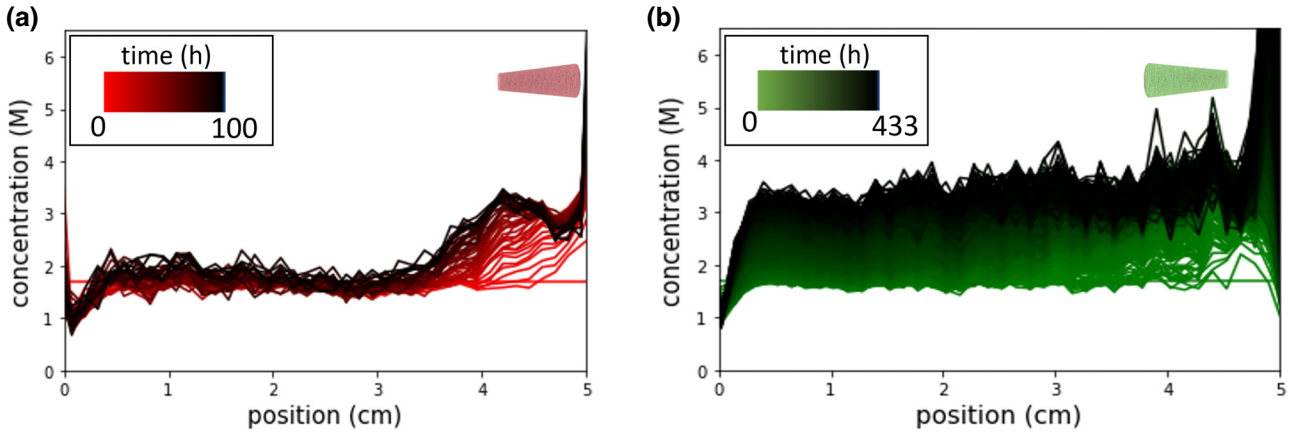

FIG. 10. Concentration (moles per liter), determined by NMR measurements, versus evaporation time for cones filled with salt solution with an initial concentration of 1.7M. (a) Large base of the cone and (b) small base as the evaporative surface. The position 0 corresponds to the bottom of the sample, the position 5 corresponds to the top evaporative surface.

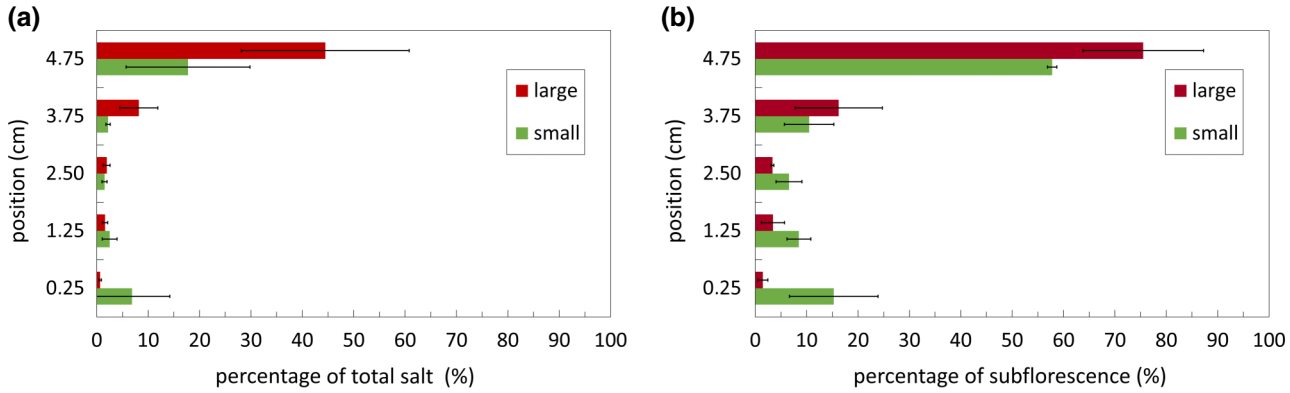

FIG. 11. Bar plot depicting the percentage of detected salt as subflorescence versus the height of the cone-shaped sample (0 corresponding to the bottom of the sample) filled initially with a 10-wt % aqueous NaCl solution after drying with the large base facing upward (red bars) and with the small base facing upward (green bars). (a) Percentage of total salt introduced in the experiments and (b) percentage of the total subflorescence.

exponential-decay regime. The liquid front loses contact with the top surface and sinks into the cone itself, causing salt precipitation as subflorescence. The Péclet number drops even further at this point to almost zero (Fig. 9) and no change in the efflorescence can be seen anymore [Fig. 4(a) and Video 1].

At the end of the drying experiments, the amount of salt left as subflorescence in the stone was quantified by our measuring the conductivity of the salt solutions made by our dissolving the salt inside different slices of the stone samples. For that, the dried cone-shaped samples were cut into five pieces. The top 0.5 cm and the bottom 0.5 cm of the cones were cut off and three pieces of 1 cm were cut from the middle. This was done without our using water during cutting to prevent the subflorescent salt from dissolving. Because of the 0.2-cm diameter of the saw, in total 1 cm of the sample was lost in the process. The pieces of the cones were placed in 50 ml of Milli-Q water for 24 h. After this time, the conductivity of the solutions was measured and compared with the calibration curve. The latter was constructed by our measuring the conductivity of seven NaCl solutions with different concentrations. In this way, we could estimate the amount of salt left in the cone at different positions and the percentage of the total salt detected as subflorescence at different positions inside the cone (Fig. 11). The bar plots depicting the percentage of salt ending up as subflorescence inside the cone after the experiment [Fig. 11(a)] show that when the large base is facing upward $(56.9 \pm 14.9)\%$ of the salt ends up as subflorescence, whereas for the small base facing upward, $(31.1 \pm 21.6)\%$ remains inside the cone. Also from the bar plots in Fig. 11 we can see that apart from the top sublayer, the amount of salt is more evenly spread over the cones that dried with the small surface facing upward, which is in good agreement with the NMR concentration profiles (Fig. 10). In Fig. 11(b) it can be also seen that most of the subflorescence ends up around 1.5 cm beneath the evaporative surface area of the cones for both geometries. This corresponds to the same height where the second concentration peak in the NMR profiles can be seen (Fig. 10). Clearly, when the large base is facing upward, there is continuity between the salt efflorescence and subflorescence. In some way, the salt crystals and the grains of the stone intertwine to create a strong adhesion, making the salt hard to remove [Figs. 6(b) and 6(e)]. These observations are in excellent agreement with real damaged artworks with holes and cracks such as the tiles in the Palacio de Cristal in Madrid shown in Fig. 1(b), where more salt efflorescence is observed in the smaller delaminated areas of the glaze than in the larger ones next to it. For future research it would be useful to study a method to predict the amount of efflorescence and subflorescence in real artworks by measuring the drying rate and by real-time calculation of the Péclet number. This opens novel routes for the conservation and restoration of art, buildings, and cultural heritage.

IV. CONCLUSION

In conservation we are faced, in general, with situations where salt crystallization is seen in complex situations at the surface of layered or/and composite materials. Here we show that the mechanism of efflorescence and subflorescence formation of salt is not only affected by the evaporation conditions and material properties but is also largely affected by the evaporative surface area for a given material. By using truncated cone–shaped samples, we have investigated the asymmetrical liquid flow for a given volume of salt solution at a given concentration. We show the impact of fluid transport from a larger region beneath the surface to a smaller, localized evaporative area by providing more insight into the effect of the Péclet number on the difference in crystallization seen.

The small surface-area-to-volume ratio shows an exponential drying regime after a very short constant-rate period and a Péclet number (characteristic of the advection-to-diffusion ratio of ions) greater than 1 for the whole duration of the drying. The advection of ions being the dominant transport leads to a high concentration gradient towards the evaporative surface. As a consequence, a large amount of salt efflorescence as porous clusters of an assembly of microcrystalites forms from the early stage of evaporation and will cover the surface during drying. The efflorescence shows weak adhesion to the stone due to the formation of localized salt-microcrystal pillars beneath the salt crust. These are formed when the salt crust loses hydraulic contact with the top surface of the salt crust. The salt pillars collectively induce a weak adhesion of the whole salt crust. Consequently, the salt crust can easily be removed from the surface of the sample. In contrast, a high evaporative-surface area-to-volume ratio exhibits first a constant-drying-rate regime for a long period followed by an exponential-decay period. In this situation, although the initial Péclet number is greater than 1, it drops gradually below 1 with the decrease of moisture content, leading to a more-even ion distribution beneath the surface. Consequently, salt precipitation occurs both at the top surface and also in the subsurface region, while keeping the porous network of the samples open. The subflorescence is found to be more interlaced with the efflorescence salt, leading to strong adhesion to the porous materials and making the salt hardly removable. Our findings are relevant in terms of predicting damage over time, as what is reported in this paper clearly shows that as the damaged area increases, the risk of subsurface crystallization becomes higher, which in turn can lead to greater deterioration due to crystallization pressure and cracking. The results give an insight into the dynamics of materials with aging and especially give more insight into the reason for the self-amplifying evolution of damage over time. One might think that a small evaporative surface would lead to greater crystallization beneath the surface as subflorescence and prevent salt from escaping from the porous medium. Surprisingly, our results show exactly the opposite; with the enlargement of the evaporative surface area, the percentage of subflorescence increases. We explain the reason for this behavior by our NMR measurements of ion transport in the liquid with flow and during evaporation and the estimation of the Péclet number. With the increase of the evaporative surface area, the ratio between ion advection and ion diffusion changes towards more ion diffusion, explaining the increase of more crystallization in the subsurface.

The understanding of these principles could help to elucidate the mechanisms behind the growth of different types of efflorescence for the same salt in relation to the evaporation rate, asymmetrical fluid flow, and resulting ion transport in a porous medium. The knowledge that by one knowing the evaporation rate and the Péclet number that the type of efflorescence and subflorescence is predictable and can be measured and thus tuned in real time during drying is very valuable for (art and heritage) conservation science in order to propose solutions to prevent salt damage and to develop better conservation strategies. Because in time and with water, but with ions and different surface areas as well, everything changes.

Data are available upon request.

ACKNOWLEDGMENTS

This research is part of the Joint Programming Initiative on Cultural Heritage CRYSTINART project [44]. The Joint Programming Initiative on Cultural Heritage project has received funding from the European Union's Horizon 2020 research and innovation program under Grant Agreement No. 699523. The authors thank Gertjan Bon for the fabrication of the cone-shaped samples and Gerrit Hardeman for the development of the software in the experimental setup.

L.P., N.S., and R.W. conceived the idea and designed and conceptualized the research. The method was developed by R.W., L.P., and N.S., who worked on the investigation together with F.V.d.S. R.W. and F.V.d.S. performed the experiments R.W. and F.V.d.S were responsible for the visualization. The project was administered by N.S., who supervised the research and experiments together with L.P. The original draft was written by R.W, who edited the draft together with N.S. and L.P.

The authors declare no conflict of interest.

[1] L. da Vinci, Il Codice Arundel, no. 263, folio 57r (1513), translated by E. MacCurdy.

[2] M. Matteini and A. Moles, A preliminary investigation of the unusual technique of Leonardo's mural "The Last Supper", Stud. Conserv. **24**, 125 (1979).

[3] M. Bauer, K. Fukunaga, A. Keil, F. Aramini, M. Palazzo, L. Dall'Aglio, and F. Friederich, *52nd European Microwave Conference 2022* (IEEE, Milan, Italy, 2022), p. 808, https://publica.fraunhofer.de/items/e8d5e00b-b254-4f12-b0c4-ce30b3ae289e.

[4] A. Goudie and H. Viles, *Salt Weathering Hazards* (Wiley, Chichester, 1997).

[5] A. E. Charola, Salts in the deterioration of porous materials: An overview, J. Am. Inst. Conserv. **39**, 327 (2000).

[6] N. Shahidzadeh-Bonn, J. Desarnaud, F. Bertrand, X. Chateau, and D. Bonn, Damage in porous media due to salt crystallization, Phys. Rev. E **81**, 066110 (2010).

[7] E. Doehne, Salt weathering: A selective review, Geol. Soc., London, Spec. Publ. **205**, 51 (2002).

[8] C. Price, Salt damage in porous materials: A threat to the cultural heritage, Archaeol. Int. **1**, 47 (1997).

[9] K. Linnow, L. Halsberghe, and M. Steiger, Analysis of calcium acetate efflorescences formed on ceramic tiles in a museum environment, J. Cult. Herit. **8**, 44 (2007).

[10] C. Groot, R. van Hees, and T. Wijffels, Selection of plasters and renders for salt laden masonry substrates, Constr. Build. Mater. **23**, 1743 (2009).

[11] C. M. Ferreira, L. M. Ottosen, I. V. Christensen, S. H. Brammer, and D. A. Sveegaard, in *Proceedings at XII DBMC – 12th International Conference on Durability of Building Materials and Components* (Porto Portugal, 2011), pp. 897–903.

[12] M. Coppola, T. Cristina, F. DI BENEDETTO, and M. E. A. Giordano, *Fifth International Conference on Salt Weathering of Buildings and Stone Sculptures* (TU Delft Open, Netherlands, 2021), p. 359.

[13] C. Alves, C. A. Figueiredo, J. Sanjurjo-Sánchez, and A. C. Hernández, Salt weathering of natural stone: A review of comparative laboratory studies, Heritage **4**, 1554 (2021).

[14] C. Bertolin, Preservation of cultural heritage and resources threatened by climate change, Geosci. **9**, 250 (2019).

[15] M. J. Qazi, D. Bonn, and N. Shahidzadeh, Drying of salt solutions from porous media: Effect of surfactants, Transp. Porous Media **128**, 881 (2019).

[16] N. Shahidzadeh-Bonn, S. Rafaı, D. Bonn, and G. Wegdam, Salt crystallization during evaporation: Impact of interfacial properties, Langmuir **24**, 8599 (2008).

[17] J. Desarnaud, H. Derluyn, L. Molari, S. de Miranda, V. Cnudde, and N. Shahidzadeh, Drying of salt contaminated porous media: Effect of primary and secondary nucleation, J. Appl. Phys. **118**, 114901 (2015).

[18] H. Eloukabi, N. Sghaier, M. Prat, and S. Ben Nassrallah, Drying experiments in a hydrophobic model porous medium in the presence of a dissolved salt, Chem. Eng. Technol. **34**, 1085 (2011).

[19] H. Eloukabi, N. Sghaier, S. B. Nasrallah, and M. Prat, Experimental study of the effect of sodium chloride on drying of porous media: The crusty–patchy efflorescence transition, Int. J. Heat Mass Transf. **56**, 80 (2013).

[20] F. Hidri, N. Sghaier, H. Eloukabi, M. Prat, and S. B. Nasrallah, Porous medium coffee ring effect and other factors affecting the first crystallisation time of sodium chloride at the surface of a drying porous medium, Phys. Fluids **25**, 127101 (2013).

[21] F. Li, H. Liu, H. Yang, R. Ayyamperumal, and Y. Liu, Influence of water vapor sorption of NaCl-Na_2So_4-containing mural earthen plaster and preliminary deterioration analysis, Total Environ. Res. Themes **6**, 100040 (2023).

[22] J. Desarnaud, D. Bonn, and N. Shahidzadeh, The pressure induced by salt crystallization in confinement, Sci. Rep. **6**, 30856 (2016).

[23] R. J. Flatt, F. Caruso, A. M. A. Sanchez, and G. W. Scherer, Chemo-mechanics of salt damage in stone, Nat. Commun. **5**, 4823 (2014).

[24] S. Veran-Tissoires and M. Prat, Evaporation of a sodium chloride solution from a saturated porous medium with efflorescence formation, J. Fluid Mech. **749**, 701 (2014).

[25] RILEM Technical Committees, MS-A.1 Determination of the resistance of wallettes against sulphates and chlorides, Mater. Struct. **31**, 2 (1998).

[26] R. J. Flatt, N. Aly Mohamed, F. Caruso, H. Derluyn, J. Desarnaud, B. Lubelli, R. M. Espinosa-Marzal, L. Pel, C. Rodriguez-Navarro, and G. W. E. A. Scherer, Predicting salt damage in practice: A theoretical insight into laboratory tests, RILEM Tech. Lett. **2**, 108 (2017).

[27] F. Boulogne, Cheap and versatile humidity regulator for environmentally controlled experiments, Eur. Phys. J. E **42**, 1 (2019).

[28] F. Chauvet, P. Duru, S. Geoffroy, and M. Prat, Three periods of drying of a single square capillary tube, Phys. Rev. Lett. **103**, 124502 (2009).

[29] P. Coussot, Scaling approach of the convective drying of a porous medium, Eur. Phys. J. B-Condens. Matter Complex Syst. **15**, 557 (2000).

[30] R. D. Deegan, O. Bakajin, T. F. Dupont, G. Huber, S. R. Nagel, and T. A. Witten, Capillary flow as the cause of ring stains from dried liquid drops, Nature **389**, 827 (1997).

[31] N. Shahidzadeh-Bonn, S. Rafai, A. Azouni, and D. Bonn, Evaporating droplets, J. Fluid Mech. **549**, 307 (2006).

[32] M. Dueñas Velasco, P. Duru, M. Marcoux, and M. Prat, Efflorescence fairy ring and salt centripetal colonization at the surface of a drying porous medium containing a salt solution. impact on drying curve (EuroDrying, Paris, France, 2013).

[33] N. Sghaier and M. Prat, Effect of efflorescence formation on drying kinetics of porous media, Transp. Porous Media **80**, 441 (2009).

[34] H. Salim, P. Kolpakov, D. Bonn, and N. Shahidzadeh, Self-lifting NaCl crystals, J. Phys. Chem. Lett. **11**, 7388 (2020).

[35] J. Petkovic, PhD thesis, TU Eindhoven (2005).

[36] J. Petković, H. Huinink, L. Pel, K. Kopinga, and R. Van Hees, Salt transport in plaster/substrate layers, Mater. Struct. **40**, 475 (2007).

[37] L. Pel, A. Sawdy, and V. Voronina, Physical principles and efficiency of salt extraction by poulticing, J. Cult. Herit. **11**, 59 (2010).

[38] J. A. Rard and D. G. Miller, The mutual diffusion coefficients of $NaCl - H_2O$ and $CaCl_2 - H_2O$ at 25 °C from Rayleigh interferometry, J. Solution Chem. **8**, 701 (1979).

[39] A. Pajonk, R. Saurel, and J. Andrieu, Experimental study and modeling of effective NaCl diffusion coefficients values during Emmental cheese brining, J. Food Eng. **60**, 307 (2003).

[40] A. Ghaffari and A. Rahbar-Kelishami, MD simulation and evaluation of the self-diffusion coefficients in aqueous NaCl solutions at different temperatures and concentrations, J. Mol. Liq. **187**, 238 (2013).

[41] J. Kong, Z. Bo, H. Yang, J. Yang, X. Shuai, J. Yan, and K. Cen, Temperature dependence of ion diffusion coefficients in NaCl electrolyte confined within graphene nanochannels, Phys. Chem. Chem. Phys. **19**, 7678 (2017).

[42] L. A. Rijniers, L. Pel, H. P. Huinink, and K. Kopinga, Salt crystallization as damage mechanism in porous building materials—A nuclear magnetic resonance study, Magn. Reson. Imaging **23**, 273 (2005).

[43] L. Pel, H. P. Huinink, and K. Kopinga, *IUTAM Symposium on Physicochemical and Electromechanical, Interactions in Porous Media* (Springer, Dordrecht, The Netherlands, 2005), p. 149.

[44] https://crystinart.com/.